Classically optimized variational quantum eigensolver with applications to topological phases

Ken N. Okada [1,*] Keita Osaki [2,*] Kosuke Mitarai,[1,2,3] and Keisuke Fujii[1,2,4]
[1]*Center for Quantum Information and Quantum Biology, Osaka University, Osaka 560-8531, Japan*
[2]*Graduate School of Engineering Science, Osaka University, Osaka 560-8531, Japan*
[3]*JST, PRESTO, Saitama 332-0012, Japan*
[4]*RIKEN Center for Quantum Computing, Saitama 351-0198, Japan*

(Received 7 February 2022; accepted 16 October 2023; published 8 December 2023)

The variational quantum eigensolver (VQE) is regarded as a promising candidate of hybrid quantum-classical algorithms for near-term quantum computers. Meanwhile, VQE is confronted with a challenge that statistical error associated with measurement as well as systematic error could significantly hamper the optimization. To circumvent this issue, we propose the classically optimized VQE (CO-VQE), where the whole process of optimization is efficiently conducted on a classical computer. The efficacy of the method is guaranteed by the observation that quantum circuits with up to logarithmic depth are classically tractable via simulations of local subsystems with up to quasipolynomial cost (polynomial for constant depth). In CO-VQE, we only use quantum computers to measure nonlocal quantities after the parameters are optimized. As a proof of concept, we present numerical experiments on quantum spin models with topological phases. After the optimization, we identify the topological phases by nonlocal order parameters as well as unsupervised machine learning on inner products between quantum states. The proposed method maximizes the advantage of using quantum computers while avoiding strenuous optimization on noisy quantum devices. In addition, our paper indicates that clustering technique combined with the fidelity measured on quantum computers could be useful for phase classification in condensed-matter physics.

DOI: 10.1103/PhysRevResearch.5.043217

I. INTRODUCTION

Over the past several years, quantum computers with above 50 or 100 physical qubits have been realized [1,2]. Along with that, researchers have been focused on how to utilize those noisy intermediate-scale quantum (NISQ) devices [3] to solve problems that are hard to tackle on classical computers [4–7]. They have developed various hybrid quantum-classical algorithms applicable to quantum many-body problems [8,9], combinatorial optimization [10], machine learning [11–16], and so on.

The variational quantum eigensolver (VQE) [8,9] is one of the most promising hybrid quantum-classical algorithms to solve quantum many-body problems. VQE, based on the variational principle, searches for the ground state of the target Hamiltonian with a parametrized quantum circuit used as the *Ansatz*. In VQE, one measures energy or its parameter derivatives on a quantum computer and accordingly updates variational parameters on a classical computer. One repeats this process until the energy converges to a minimum. So far, benchmark experiments using actual quantum devices have demonstrated that, with appropriate *Ansätze*, VQE could yield approximate solutions with high precision for small quantum systems, primarily, small molecules [8,17–24]. Meanwhile, it has been also revealed that the optimization process in VQE could be significantly affected by statistical error [25–28] as well as systematic error [29–33]; the former intrinsically arises from measurement on quantum circuits, whereas the latter comes from imperfect fidelity of quantum gates and readout or decoherence of quantum states. Although various techniques of error mitigation have been proposed [5,34–44], some of which have been experimentally found effective to a certain extent [19,20], it still remains an issue how to minimize adverse effect of error on computation with NISQ devices.

To alleviate the difficulty/cost in optimization in VQE, various approaches have been explored to offload parts of the optimization procedure to classical computers. Rudolph *et al.* [45] conducted classical simulation of matrix product states to obtain better parameter initialization in VQE. Cervera-Lierta *et al.* [46] proposed meta-VQE, where, for a Hamiltonian with parameters, VQE is trained from a few data points and generates initial circuit parameters fit for other data points. Similarly, in a recent work by Ceroni *et al.* [47], neural networks are trained from a few Hamiltonian parameters to output optimal variational parameters for VQE. Kottmann and Aspuru-Guzik [48] developed a class of classically tractable quantum circuits based on separable-pair approximations, which could be used as a baseline in VQE *Ansätze*. Fujii *et al.* [49] applied a divide-and-conquer method to VQE to

[*]These authors contributed equally to this work.

reduce the number of necessary qubits. This could also help to reduce the optimization cost in VQE by replacing the second stage of VQE for classical simulations such as tensor network technique.

We propose a variant of VQE that conducts the whole process of optimization on a classical computer. We term this method the classically optimized VQE (CO-VQE). By its nature, CO-VQE is free of the aforementioned errors because it does not involve a quantum computer in the optimization process. It is based on an observation that shallow depth circuits are easy to simulate when we are only interested in local observables. For Hamiltonians with only local interactions, this allows us to optimize the *Ansatz* classically without exponential computational cost. Another important observation is that, while local observables on shallow circuits are classically simulatable, nonlocal ones are not in general. Although a novel classical algorithm has been recently developed that allows one to efficiently simulate even nonlocal observables with respect to shallow circuits [50], there are some cases where quantum computers are still needed (see the discussion in Sec. II B). Therefore, we may need to run the optimized circuit on a quantum device if we wish to obtain information about nonlocal quantities. This kind of situation occurs very naturally with a quantum system which exhibits a topological phase transition, where the system Hamiltonian is local but its order parameters are global [51–53]. Another useful quantity that may have to be measured on a quantum device is the inner product between the states, which can be used for, e.g., the unsupervised clustering of states in different phases [54].

As numerical demonstrations of CO-VQE, we study two quantum spin models in which topological orders emerge; the one-dimensional (1D) cluster model [55,56] and the two-dimensional (2D) toric code model with transverse field [57–59]. CO-VQE would be practically important in 2D systems because in 1D systems, one can often obtain the ground states with high accuracy as well as evaluate nonlocal observables efficiently on classical computers using matrix product states (MPS). After optimization, we characterize the topological phases by measuring nonlocal order parameters. Moreover, for the 1D model, we identify the topological phase via another method, measurement of fidelity combined with an unsupervised machine learning. We also refer to recent similar works in Refs. [60,61].

The paper is organized as follows. First, we describe the principle of CO-VQE in Sec. II. We devote Secs. III and IV to numerical demonstrations of CO-VQE on the 1D cluster and 2D toric code models with transverse field, respectively. Finally, we summarize our results in Sec. V.

II. CLASSICALLY OPTIMIZED VARIATIONAL QUANTUM EIGENSOLVER

A. Principle of CO-VQE

In this section, we explain the premise and principle of CO-VQE. In the optimization process of the original VQE, one evaluates expectation values of operators by measurement on a quantum computer and accordingly update variational parameters on a classical computer [Fig. 1(a)]. In CO-VQE,

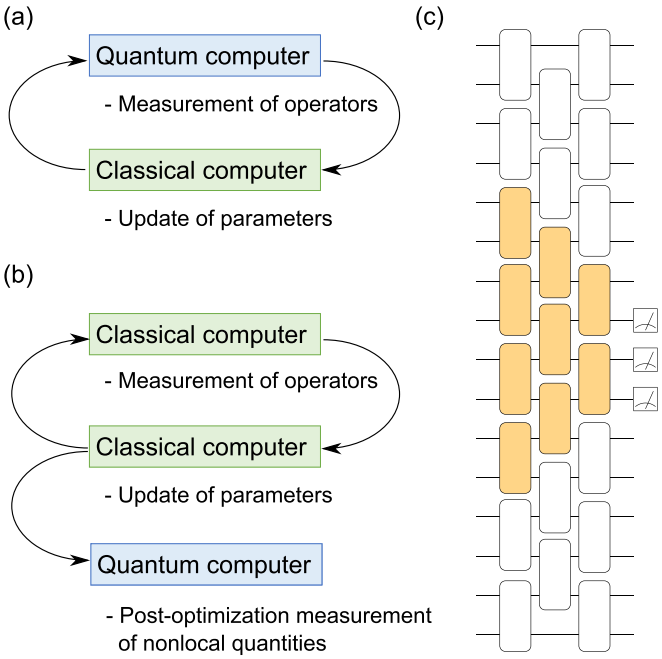

FIG. 1. Schematic diagram of (a) the original VQE and (b) CO-VQE. (c) Causal cone (orange area) in a brickwall quantum circuit.

meanwhile, one efficiently calculates the expectation values with a classical computer instead of using a quantum computer [Fig. 1(b)]. The key to the efficiency is reduction in the number of simulated qubits, thanks to the locality of causal cones in shallow-depth quantum circuits [Fig. 1(c)].

As prerequisites for CO-VQE, we suppose the following constraints on the target problem and *Ansatz*.

(i) Operators measured in the optimization process are local.

(ii) The initial state of the quantum circuit is a product state or more generally a stabilizer state.

(iii) The quantum circuit is only composed of local operations.

(iv) The quantum circuit has a constant or logarithmic depth as a function of the system size.

In many systems of interest in condensed-matter physics, the constraint (i) holds for operators composing the physical Hamiltonian. In addition, a majority of the circuit *Ansätze* proposed so far meet the constraints (ii) and (iii). The constraint (iv) allows for hardware-efficient *Ansätze* [8,18,20] as well as the Hamiltonian variational *Ansatz* [25] in spin models as we treat them in the paper. Although (iv) restricts depth of the *Ansatz*, we remark that, when one increases the system size up to, e.g., 10^3 or 10^4, in the NISQ era, polynomially scaled circuit depths are not ideal or viable due to exponential decrease in fidelity.

Under those constraints, one can classically simulate quantum circuits without suffering from exponential increase in the computational cost. As a simple example, let us consider a 1D brickwall quantum circuit applied to a product state [Fig. 1(c)]. As indicated in Fig. 1(c), measurement of a local operator on the circuit only involves a part of the qubits considering the causal cone. Therefore, it only suffices to simulate a local subsystem rather than the entire

system. When implementing a causal cone simulator, one would trace back all the gates in the opposite direction of time, judging whether or not each gate is relevant to the measurement results and adding the relevant gates to the causal cone.

The argument can be generalized to d dimensions ($d \geqslant 1$). Let N be the number of qubits of the entire system. Suppose we calculate the expectation value of a local observable $\mathcal{O}$ with respect to a quantum circuit with depth l. Assuming that $\mathcal{O}$ is described as a sum of m k-body Pauli operators, the maximal number of qubits among the causal cones corresponding to m Pauli operators, M, is estimated as $M = O(kl^d)$. Hence, evaluation of the observable $\mathcal{O}$ costs $O(m2^{kl^d})$, whereas it costs $O(m2^N)$ when one simulates the entire system. In the case where $\mathcal{O}$ is the Hamiltonian, considering $m = O(\mathrm{poly}(N))$ ($O(N)$ in typical spin models), the simulation assisted by causal cones can be performed efficiently as long as the depth l is up to logarithmic with respect to N. More specifically, the simulation costs polynomial time when l is constant for any d or logarithmic for $d = 1$ and quasipolynomial time when l is logarithmic for $d \geqslant 2$. Importantly, this technique enables us to classically simulate systems with more qubits than current computers could afford to simulate, e.g., $N \approx 100$ as long as M is sufficiently small.

One might think that the efficient simulatability of low-depth quantum circuits for local observables is limited to cases where the initial state is a product state. In fact, however, it holds as long as the initial state is a stabilizer state. Supposing that U represents the quantum circuit, $U^\dagger \mathcal{O} U$ can be decomposed into $O(m4^{kl^d})$ (kl^d)-body Pauli operators. Since expectation values of Pauli products with respect to a stabilizer state can be efficiently calculated on classical computers, one can efficiently simulate the expectation value of the local observable when l is up to logarithmic. In the numerical simulations in Secs. III and IV, we use stabilizer states as the initial state of the *Ansatz*.

The argument above raises a question; once the entire optimization is conducted on a classical computer, in what cases does one benefit from using a quantum computer? The answer could be in cases where one conducts measurement of nonlocal quantities [Fig. 1(b)]. One case which necessitates such measurements could be characterization of topological orders [51–53] emergent in certain quantum spin models. Since order parameters of topological phases are nonlocal, it may be necessary to measure them on a quantum device to explicitly tract topological orders. Another case that we consider here is measurement of fidelity, the absolute value of the inner product between two quantum states. Fidelity is useful to detect quantum phase transitions, especially when one does not know an apparent form of order parameter [62,63]. We may also need to evaluate it on a quantum device due to its globality.

B. Discussion of classical simulatability

In this section, we discuss classical simulatability of constant-depth quantum circuits in more depth. In the previous section, we have shown that measurement of nonlocal operators with respect to constant-depth circuits cannot be efficiently simulated by the causal cone technique. However, it does not mean that nonlocal operators with constant-depth circuits are not classically simulatable.

Recently Bravyi, Gosset, and Movassagh have developed a classical randomized algorithm that can efficiently simulate even nonlocal operators for 2D circuits of constant depth [50]. Since the algorithm is the first one among the three they introduced in the paper, we call the algorithm BGM1 hereafter. BGM1 simulates a N-body product of single-qubit observables O_j ($\|O_j\| \leqslant 1$) with respect to a 2D quantum circuit with local operations (U) within an additive error δ. Here the expectation value $\langle 0^N | U^\dagger O_1 \otimes \cdots \otimes O_N U | 0^N \rangle$ is estimated via Monte Carlo sampling. The key procedure is that the 2D grid of qubits is divided into 1D strips based on causal cone considerations. On each strip, the amplitudes of the corresponding parts of sampled bit strings are computed by state vector simulations on $m(r) = 6r^2 - r + 1$ qubits, with range r, roughly speaking, the largest radius of N causal cones with a single qubit at the vertex. In total, the run time scales as $O(Nr^2\delta^{-2})2^{m(r)}$. Therefore, the algorithm takes linear time for constant depth and quasipolynomial time for logarithmic depth (assuming r is proportional to circuit depth l). We note that, for a three-dimensional case, BGM1 takes subexponential time even for constant depth with the run time scaled as $O(Nr^3\delta^{-2})2^{m(r)N^{1/3}}$.

In terms of computational complexity, it seems that BGM1 can replace quantum computers for nonlocal measurement on 2D constant-depth circuits. However, a caveat is that not every operator can be classically simulated with respect to constant-depth circuits. To see this, let us consider measurement-based quantum computation (MBQC) using the cluster state on the 2D square lattice, which is known to be universal [64,65]. The cluster state can be prepared by applying four layers of CZ gates to the zero state. Then arbitrary quantum computation can be performed by a certain pattern of single-qubit measurements on the cluster state. As a result, MBQC on the cluster state can be described as measurement on the constant-depth quantum circuit. If the expectation value of an arbitrary operator with respect to constant-depth circuits were classically simulatable, MBQC and hence universal quantum computation could be simulated on classical computers. This is not supposed to be true obviously. Therefore it is not true that an arbitrary operator with respect to constant-depth circuits can be classically computed. Indeed, one can see that BGM1 cannot be applied to the above case because of the normalization factors associated with measurement (see the Appendix).

In Sec. IV, we consider nonlocal measurements on the states generated by applying constant-depth circuits to the toric code state after the optimization in CO-VQE. Those measurements cannot be efficiently simulated by the causal cone technique presented in Sec. II A. Although we cannot give a proof that the measurements are not classically simulatable, we can at least say that BGM1 is not applicable to the case considered. This is because the toric code state cannot be deterministically prepared using quantum circuits of constant depth. Importantly, local operators can be classically simulated by our causal cone technique since the toric code state is a stabilizer state (see Sec. II A). Those properties make the case in Sec. IV suitable to CO-VQE.

C. Numerical simulations

In Secs. III and IV, we present proof-of-concept demonstrations of CO-VQE on quantum spin models with topological phases. First, in Sec. III, we study the 1D cluster model with transverse field. However, in 1D systems, one can efficiently evaluate nonlocal observables on a classical computer if the circuit has a constant or logarithmic depth. In that sense, CO-VQE is expected to provide practical importance in 2D systems. In Sec. IV, we treat the 2D toric code model with transverse field, where classical simulations of nonlocal operators are not feasible with BGM1 as described in Sec. II B.

We simulate quantum circuits using QULACS [66] and optimize variational parameters using the BFGS method implemented in the SCIPY library [67]. In Sec. III A, we conduct optimization sequentially from $J = 0$ to 2.0 in increments of $\Delta J = 0.1$, where we set initial parameters for $J = J'$ at the optimized values for $J = J' - \Delta J$. Here we add a small random deviation to initial parameters to facilitate a move from the initial point in the parameter space. In Sec. III C, at fixed J_2, we similarly run optimization from $J_1 = 0$ to 1.6 in increments of ΔJ while setting initial parameters for $J_1 = J_1'$ at the optimized values for $J_1 = J_1' - \Delta J$ with a small random deviation added. At $J_1 = 0$, we set initial parameters for $J_2 = J_2'$ at the optimized ones for $J_2 = J_2' - \mathrm{sgn}(J_2)\Delta J$ with a small random deviation. In Sec. III C, we tested ten random deviations and chose the one with the best convergence to the exact energies. Meanwhile, in Sec. IV, we tested ten (twenty) runs with different random initial parameters for $D = 1, 2, 3$ ($D = 4, 5$) and selected the best one for each h_z.

We also perform exact diagonalization (ED) to obtain reference values. For clustering, we employ SCIKIT-LEARN [68]. We note that our studies are restricted to a classically tractable number of qubits ($N \leqslant 25$) so that we could simulate nonlocal measurements, which would be conducted on quantum computers in actual usage of CO-VQE.

III. TRANSVERSE-FIELD CLUSTER MODEL

A. Nonlocal order parameter

In this section, we study the 1D cluster model with transverse field [55]. We consider an N-qubit chain with open boundary condition, where the Hamiltonian reads

$$\mathcal{H}_{\mathrm{cluster}} = -\sum_{i=2}^{N-1} K_i - J\sum_{i=1}^{N} X_i. \tag{1}$$

We define the stabilizer K_i as $K_i = Z_{i-1}X_iZ_{i+1}$. For $J = 0$, the ground state of the model is in a symmetry-protected topological (SPT) phase [52,53] and called the cluster state [64]. The state is characterized with eigenvalues of K_i being equal to 1 for all i. The model is exactly solvable because it can be mapped to the transverse-field Ising model via a nonlocal transformation [55]. The exact solution tells us that as J increases from zero, the cluster state transitions to a trivial phase at $J = 1$. The order parameter characterizing the phase transition is a product of the stabilizers represented as

$$\Omega = \left\langle \prod_{k=1}^{\lfloor \frac{N-1}{2} \rfloor} K_{2k} \right\rangle. \tag{2}$$

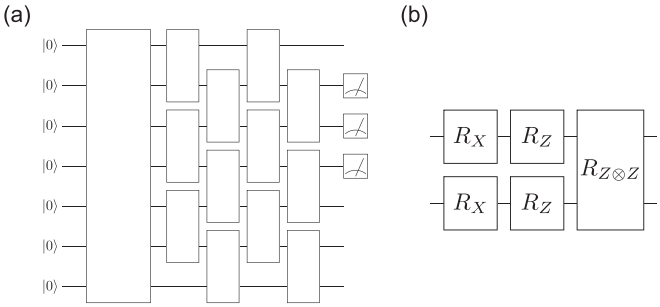

FIG. 2. (a) Brickwall quantum circuit used as the *Ansatz* of CO-VQE for the transverse-field cluster model. The leftmost block corresponds to a circuit that generates the cluster state. (b) Quantum operations comprising a single brick in (a).

The cluster state corresponds to $\Omega = 1$, whereas the trivial phase has $\Omega = 0$ [55]. We remark that the order parameter Ω is a nonlocal observable.

We study the ground state of $\mathcal{H}_{\mathrm{cluster}}$ by CO-VQE. We use a brickwall quantum circuit applied to the cluster state [Fig. 2(a)] as the *Ansatz*. The *Ansatz* and Hamiltonian meet four conditions for CO-VQE listed in Sec. II. Note that the cluster state is a stabilizer state. As shown in Fig. 2(b), each brick is composed of four single-qubit rotations and one two-qubit rotation with independent variational parameters. We define the depth of the circuit l_1 as the number of brick layers [$l_1 = 4$ in Fig. 2(a)]. Importantly, the *Ansatz* corresponds to the Hamiltonian variational *Ansatz* [25]. This guarantees that the *Ansatz* can generate the exact solution when $l_1 \to \infty$. As described in Sec. II A, in the optimization process of CO-VQE, we only simulate relevant qubits dictated by the causal cone [Fig. 1(c)] to evaluate expectation values of the local terms in $\mathcal{H}_{\mathrm{cluster}}$.

First, we study the phase transition by explicitly measuring the nonlocal order parameter Ω. For each value of J ($0 \leqslant J \leqslant 2$), we optimize variational parameters and then compute Ω. In Figs. 3(a) and 3(b), we show J dependence of the ground state energy E and Ω, respectively, for $N = 16$ and $l_1 = 4$ as well as those calculated by ED. As expected, the order parameter Ω of ED [Fig. 3(b)] points to the phase transition at $J \approx 1$. Figures 3(a) and 3(b) show that both the energy and order parameter of CO-VQE agree well with those of ED. We note that Ω of CO-VQE shows a slightly steeper decline at the phase transition than that of ED [Fig. 3(b)], which might be attributed to limitation of expressibility in the low-depth *Ansatz*. The result implies that the brickwall circuit of even a low depth [Fig. 2(a)] can capture a broad range of quantum states including the cluster state and trivial state at the end points.

B. Clustering on fidelities

Next, as another approach to detect the phase transition, we use fidelity for unsupervised machine learning. Fidelity measures similarity between two quantum states $|\Psi\rangle$ and $|\Phi\rangle$, and it is defined as

$$F = |\langle\Phi|\Psi\rangle|. \tag{3}$$

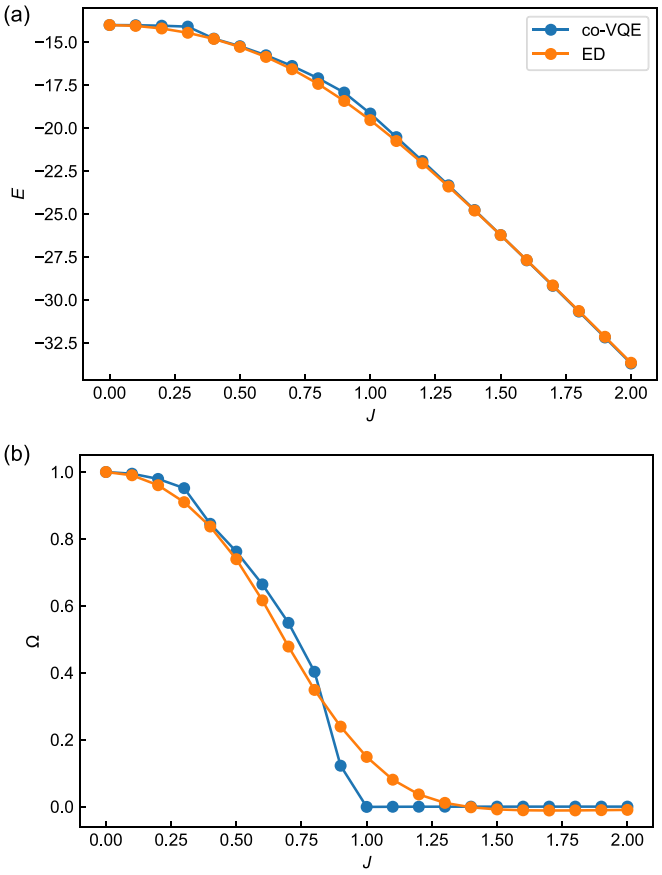

FIG. 3. J dependence of (a) the energy E and (b) nonlocal order parameter Ω in Eq. (2) of the ground states obtained by CO-VQE on the transverse-field cluster model with the Hamiltonian $\mathcal{H}_{\text{cluster}}$ in Eq. (1). The blue (orange) points show the data of CO-VQE (ED). In CO-VQE, we set the depth of the *Ansatz* as $l_1 = 4$. The calculations are done for $N = 16$.

In the last decade and a half, researchers in condensed-matter physics have found out that fidelity is a useful tool to detect quantum phase transitions [62,63], especially when one does not have information of order parameters. This stems from the property that the fidelity F equals almost 1 between quantum states within the same phase, and zero between states in different phases. Although in the thermodynamic limit one should employ other relevant quantities such as fidelity per site [60,69,70] or fidelity susceptibility [71] to avoid the orthogonality catastrophe [72], in the following we can safely rely on fidelity because we only treat small-size systems.

We compute fidelities between the optimized states for different values of J. In actual usage of quantum computers, one can evaluate the fidelity by measuring the probability of $|0\rangle^{\otimes N}$ on the circuit shown in Fig. 4. One can readily see that the fidelity is a nonlocal quantity because one needs to measure all the qubits. Figure 5(a) shows the color plot of fidelity $|\langle\Psi(J')|\Psi(J)\rangle|$. The top row of the color plot in Fig. 5(a) shows that as J increases, the fidelity $|\langle\Psi(J' = 2.0)|\Psi(J)\rangle|$ steeply arises around $J = 1$. Therefore one can speculate that a phase transition seems to take place around $J = 1$.

To confirm the observation, we conduct clustering on the data set of fidelity for phase classification [Fig. 5(a)]. Here,

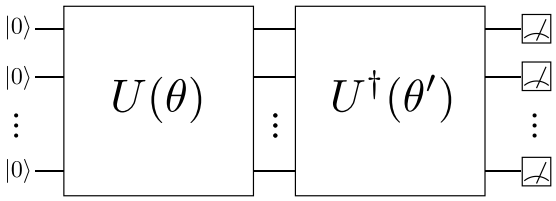

FIG. 4. Quantum circuit for measuring the square of fidelity $F = |\langle 0|^{\otimes N} U^\dagger(\theta')U(\theta)|0\rangle^{\otimes N}|$.

we apply the spectral clustering method with the number of clusters fixed at 2 while using the fidelity as affinity between data points. As a consequence, we obtain two phases as shown in Fig. 5(b); one corresponds to $0 \leqslant J \leqslant 0.9$ (SPT phase), and the other to $1 \leqslant J \leqslant 2$ (trivial phase). The result is consistent with the exact phase diagram. We emphasize that clustering allows us to detect the phase transition without prior knowledge of the order parameter Ω. Our clustering analysis contrasts with recent studies that have proposed similar methods for classifying phases based on measurement of fidelity in conjunction with classical machine learning [60,61], both of which employ supervised machine learning.

C. Adding Ising interactions

We also study the phase diagram when Ising interactions are added to $\mathcal{H}_{\text{cluster}}$. The Hamiltonian that we consider here reads

$$\mathcal{H}_{\text{Ising cluster}} = -\sum_{i=2}^{N-1} K_i - J_1 \sum_{i=1}^{N} X_i - J_2 \sum_{i=1}^{N-1} X_i X_{i+1}. \quad (4)$$

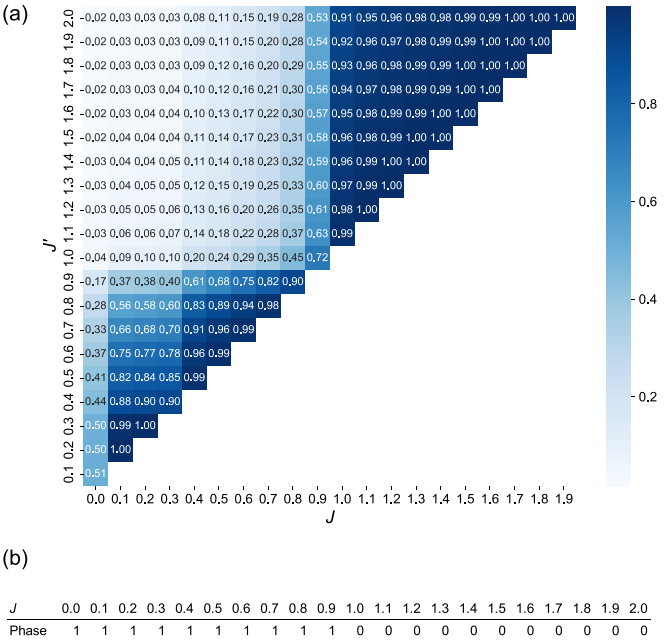

FIG. 5. (a) Color plot of the fidelity between the states optimized by CO-VQE for different values of J. (b) Phase classification by spectral clustering on the data set in (a). Phase 1 corresponds to the SPT phase and phase 0 corresponds to the trivial phase.

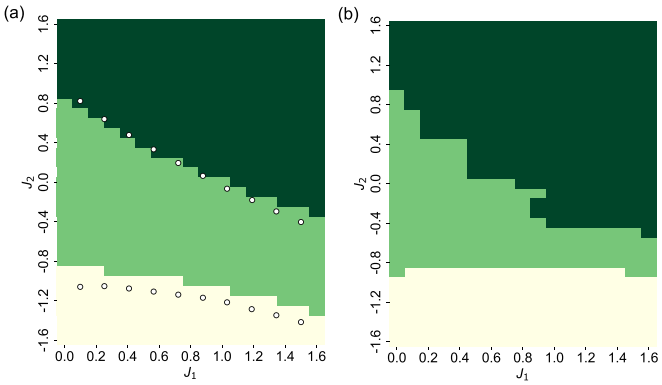

FIG. 6. Phase classification by clustering on the fidelities computed by (a) ED and (b) CO-VQE with $l_1 = 4$ on the transverse-field cluster model with Ising interactions of the Hamiltonian $\mathcal{H}_{\text{Ising}-\text{cluster}}$ in Eq. (4). The dark green, light green, and yellow regions correspond to the ferromagnetic, SPT, and antiferromagnetic phases. The calculations are done for $N = 11$. The circles in (a) stand for the phase boundaries computed by the infinite-size DMRG calculations in Ref. [56].

For each value of J_1 and J_2 ($0 \leqslant J_1 \leqslant 1.6$, $-1.6 \leqslant J_2 \leqslant 1.6$), we compute the ground state by ED as well as CO-VQE using the same *Ansatz* in the previous sections.

First, we calculate the fidelities between the ground states obtained by ED for different values of (J_1, J_2) and conduct spectral clustering with the number of clusters fixed at 3. As shown in Fig. 6(a), the whole parameter space is classified into the SPT phase (light green), ferromagnetic phase (dark green), and antiferromagnetic phase (yellow). In Fig. 6(a), the white circles represent the phase boundaries computed by the infinite-size DMRG calculations in Ref. [56]. We can observe that our clustering based on ED agrees well with those calculations. We note that the slight difference in the phase boundaries between the two results could be attributed to the small size in our calculations.

We also conducted clustering based on CO-VQE with $l_1 = 4$ as in Sec. III B. Figure 6(b) indicates that the classification overall reproduces that for ED, although the phase boundary deviates from ED [Fig. 6(a)]. This is probably due to insufficient accuracy of the solutions in CO-VQE. We expect that the discrepancy would be reduced as l_1 increases.

IV. TRANSVERSE-FIELD TORIC CODE MODEL

While we have considered the 1D model in the previous section, classical approaches using MPS or the multiscale entanglement renormalization *Ansatz* (MERA) are in many cases sufficient for 1D models. In this section, we study the toric code model with transverse field as a nontrivial example in two dimensions. The model is defined on a square array of $N = L^2 + (L-1)^2$ (L: linear dimension) qubits with open boundary conditions as shown in Fig. 7. The Hamiltonian reads

$$\mathcal{H}_{\text{toric}} = -\sum_s A_s - \sum_p B_p - h_z \sum_{i=1}^{N} Z_i, \tag{5}$$

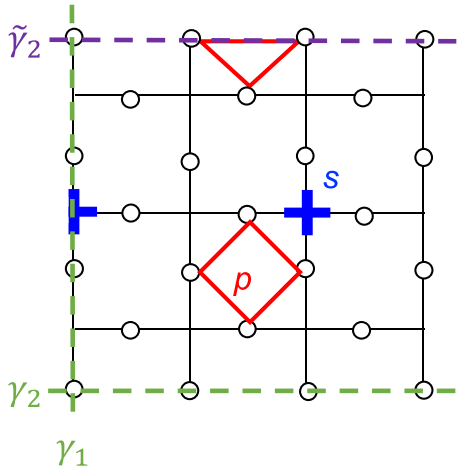

FIG. 7. Square array of qubits (open circle) with $L = 4$ for the toric code model.

where A_s and B_p are stabilizers defined as $A_s = \prod_{i \in s} X_i$ and $B_p = \prod_{i \in p} Z_i$ for each square s and plaquette p (Fig. 7), and h_z represents strength of the transverse field. For $h_z = 0$, the ground states are toric code states with a nontrivial topology [51]. They are characterized with eigenvalues of A_s and B_p being equal to 1 for all s and p, which are twofold degenerate in our setting of boundary conditions. These twofold ground states are distinguished by eigenvalues of a logical operator L_Z, defined as $L_Z = \prod_{i \in \gamma_1} Z_i$ (Fig. 7). With application of h_z, quantum Monte Carlo calculations revealed that the toric code state undergoes a topological transition at $h_z = 0.328\,474(3)$ in the thermodynamic limit [57–59].

Below we study the model by CO-VQE. We use the Hamiltonian variational *Ansatz* [25] in a more explicit form than in Sec. III. The *Ansatz* is expressed with variational parameters β_l and γ_l as

$$|\Psi\rangle = \prod_{l=1}^{D} \left[e^{-i\beta_l \mathcal{H}^0_{\text{toric}}} e^{-i\gamma_l \mathcal{H}^1_{\text{toric}}} \right] |\Psi(L_Z = 1)\rangle, \tag{6}$$

where both $\mathcal{H}^0_{\text{toric}}$ and $\mathcal{H}^1_{\text{toric}}$ are parts of $\mathcal{H}_{\text{toric}}$ defined as $\mathcal{H}^0_{\text{toric}} = -\sum_s A_s - \sum_p B_p$ and $\mathcal{H}^1_{\text{toric}} = -h_z \sum_{i=1}^{N} Z_i$. The initial state $|\Psi(L_Z = 1)\rangle$ represents the toric code state with the eigenvalue of L_Z being equal to 1, which is the exact ground state of $\mathcal{H}_{\text{toric}}$ with $h_z = 0$. The Hamiltonian and *Ansatz* satisfy four constraints for CO-VQE listed in Sec. II.

The reason why we set the toric code state as the initial state is because topologically ordered states cannot be generated from a product state with a constant depth circuit. By doing so, one can study the region belonging to the same topological phase with a constant-depth quantum circuit. Furthermore, one could also reach the phase transition with a logarithmic depth, considering that highly entangled 2D states are generated with the branching MERA with $O(\log N)$ depth [73]. Indeed, for 1D systems, critical properties of phase transitions have been discussed with log-depth MERA. A preparation of the toric code state $|\Psi(L_Z = 1)\rangle$ has been discussed in the context of quantum error correction. More precisely, the syndrome measurements for A_s project a product state $|0\rangle$ onto the toric code state $|\Psi(L_Z = 1)\rangle$. The

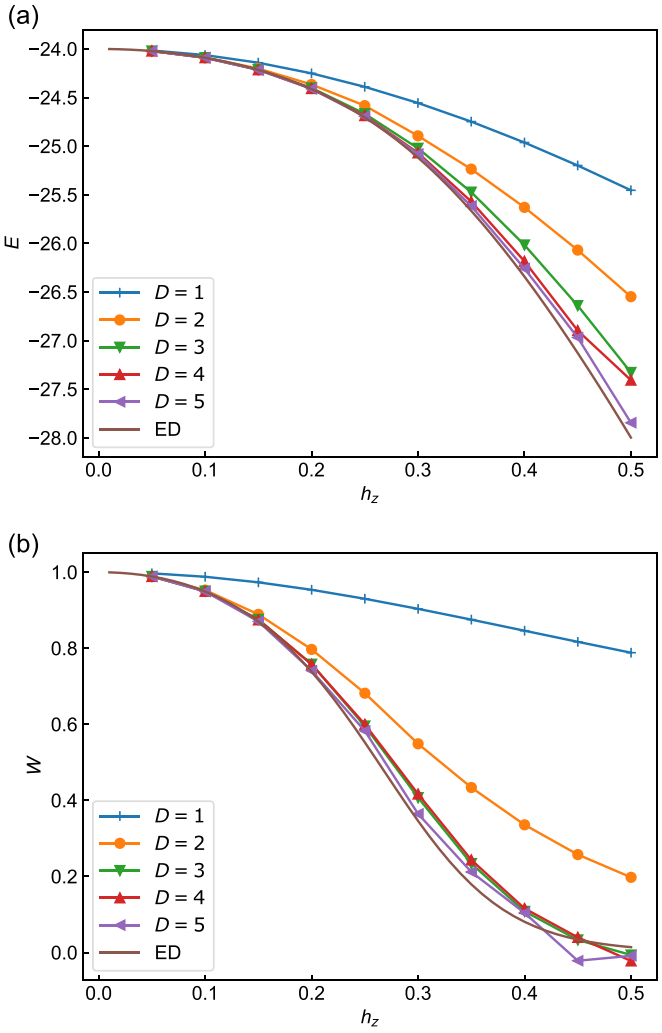

FIG. 8. h_z dependence of (a) the energy and (b) nonlocal order parameter W in Eq. (7) of the ground states obtained by CO-VQE on the transverse-field toric code model with the Hamiltonian $\mathcal{H}_{\text{toric}}$ in Eq. (5). The purple line shows the data of ED. The calculations are done for $L = 4$ ($N = 25$).

randomness of the measurement outcomes can be treated classically by updating the Pauli frame and rewriting the state and operations in an appropriate basis.

To tract the topological order, we evaluate the Wilson loop operator W [74], which we define as (Fig. 7)

$$W = \prod_s A_s = \prod_{i\in\gamma_2,\tilde{\gamma}_2} X_i. \tag{7}$$

In Figs. 8(a) and 8(b), we present h_z dependence of the energy E and nonlocal order parameter W, respectively, calculated by CO-VQE together with those of ED. The calculations are done for $L = 4$ ($N = 25$). The loop operator W computed by ED [Fig. 8(b)] shows that the toric code state gradually transitions to a trivial state as h_z increases up to 0.5. Figure 8(a) shows that the energy of CO-VQE becomes lower as the depth D increases and nearly overlaps with that of ED for $D = 5$. With regard to W, the result of CO-VQE almost replicates that of ED with a lower depth ($D = 3$) [Fig. 8(b)]. As mentioned earlier, we expect that one could also reach the phase transition in the thermodynamic limit using a log-depth circuit.

Our calculations indicate that the *Ansatz* with the toric code state as the initial state is effective. It may describe the ground states for small external field with a constant depth as well as the phase transition with a logarithmic depth. Although we restricted ourselves into a simulatable number of qubits in the calculations above, CO-VQE would be beneficial for the current scale of NISQ computers, i.e., $N = 100$–200. In the transverse-field toric code model, the maximal number of qubits among all the causal cones for evaluation of the energy is represented as $M = 4(D+1)^2$. Therefore, classical optimization would be possible up to $D = 2$ by using supercomputers [1,75] or potentially for $D = 3, 4$ by tensor network simulations on high performance computers [76–81]. If one intends to increase the depth even more, one needs to conduct optimization on quantum computers, but even in that case, CO-VQE for a smaller depth would help one to determine the initial parameters for the original depth and thus reduce the risk of being trapped at suboptimal solutions.

V. CONCLUSION

In this paper, we propose CO-VQE, a variant of VQE that is more reliant on classical computers. In CO-VQE, assuming locality of the Hamiltonian and constant (logarithmic) depth of the *Ansatz*, the whole process of optimization is efficiently conducted on a classical computer with a polynomial (up to quasipolynomial) cost. The efficiency of the classical optimization comes from exponential reduction in simulation costs by virtue of causal cones in quantum circuits. Compared to the original version of VQE, CO-VQE has an advantage that its optimization process is by definition free of statistical or systematic error inherent in quantum hardware.

CO-VQE does not exclude opportunities to benefit from quantum devices; one may need to rely on them to measure global quantities such as nonlocal order parameter and fidelity after the optimization. As a proof of concept for our method, we present numerical simulations on 1D and 2D quantum spin models with topological phases. First, we solve the 1D cluster model by CO-VQE. We detect the topological phase transition by evaluating the nonlocal order parameter. In addition, we demonstrate that even without prior knowledge of the order parameter, we could also identify the phases by applying clustering technique to fidelity. Then, given that the ground states and nonlocal observables in 1D models are often achievable by classical computers, we also study the 2D toric code model with CO-VQE. We find that the *Ansatz* initiated from the toric code state works well. The important thing is that it may cover the region within the topological phase with a constant depth and reach the phase transition with a logarithmic depth. This leads to an expectation that we may derive advantages from quantum computers if we conduct CO-VQE using a real quantum device for larger system sizes.

We expect that because of its error immunity in the optimization process, CO-VQE may have more potential than the original VQE to leverage NISQ devices to solve quantum many-body problems. Our numerical experiments also

indicate potential usefulness of unsupervised phase classification based on the fidelities measured on quantum computers.

ACKNOWLEDGMENTS

We acknowledge Hiroshi Ueda for his valuable comment. K.M. is supported by Japan Science and Technology Agency (JST) PRESTO Grant No. JPMJPR2019 and Japan Society for the Promotion of Science KAKENHI Grant No. 20K22330. K.F. is supported by JST ERATO Grant No. JPMJER1601 and JST CREST Grant No. JPMJCR1673. This work is supported by Ministry of Education, Culture, Sports, Science, and Technology Quantum Leap Flagship Program (MEXTQLEAP) Grants No. JPMXS0118067394 and No. JPMXS0120319794. We also acknowledge support from JST COI-NEXT program Grant No. JPMJPF2014.

APPENDIX: EXPONENTIAL COST OF SIMULATING MBQC BY BGM1

In this Appendix, we explain that it takes exponential time to classically simulate MBQC using the cluster state on the square lattice [64,65] by employing BGM1 [50].

Let us denote the cluster state on the square lattice as $|\psi_{\rm cl}\rangle$. In the scheme of MBQC, as $|\psi_{\rm cl}\rangle$ is a universal resource state, arbitrary quantum circuit operation $V|0^N\rangle$ can be generated by adaptive single-qubit measurements on $|\psi_{\rm cl}\rangle$ [65]. This is represented by

$$V|0^N\rangle = \sqrt{2^M}\prod_{i\in\mathcal{S}_{\rm m}} P_i|\psi_{\rm cl}\rangle \tag{A1}$$

with P_i a projection operator onto an appropriate basis, $\mathcal{S}_{\rm m}$ the subset of qubits measured, and M the number of elements in $\mathcal{S}_{\rm m}$. Then the expectation value of a single-qubit observable A_j ($\|A_j\| \leqslant 1$, $j \notin \mathcal{S}_{\rm m}$) with respect to $V|0^N\rangle$ is

$$\alpha = \langle 0^N|V^\dagger A_j V|0^N\rangle \tag{A2}$$

$$= 2^M\langle\psi_{\rm cl}|A_j\prod_{i\in\mathcal{S}_{\rm m}} P_i|\psi_{\rm cl}\rangle. \tag{A3}$$

We consider employing BGM1 to simulate the right-hand side of Eq. (A3). BGM1 is a sampling-based algorithm that efficiently simulates $\langle 0^N|U^\dagger O_1\otimes\ldots\otimes O_N U|0^N\rangle$ with any single-qubit observable O_j ($\|O_j\|\leqslant 1$) and any 2D quantum circuit U of range r within an additive error δ [50]. The simulation costs $O(Nr^2\delta^{-2})2^{m(r)}$ with $m(r) = 6r^2-r+1$. Noting that $|\psi_{\rm cl}\rangle$ is generated by applying four layers of CZ gates and that $\|P_i\| = 1$, one can approximate $\beta = \langle\psi_{\rm cl}|A_j\prod_{i\in\mathcal{S}_{\rm m}} P_i|\psi_{\rm cl}\rangle$ by utilizing BGM1. The approximate value $\tilde{\beta}$ satisfies $|\tilde{\beta}-\beta| < \delta$. Since $\alpha = 2^M\beta$ holds from Eq. (A3), α is approximated as $\tilde{\alpha} = 2^M\tilde{\beta}$, leading to $|\tilde{\alpha}-\alpha| < 2^M\delta$. Combined with $M = O(N)$, the equation indicates that one would need exponentially small δ with respect to N to approximate α with an additive error. This means that it would take exponential time to simulate MBQC by using BGM1.

[1] F. Arute, K. Arya, R. Babbush, D. Bacon, J. C. Bardin, R. Barends, R. Biswas, S. Boixo, F. G. S. L. Brandao, D. A. Buell, B. Burkett, Y. Chen, Z. Chen, B. Chiaro, R. Collins, W. Courtney, A. Dunsworth, E. Farhi, B. Foxen, A. Fowler *et al.*, Quantum supremacy using a programmable superconducting processor, Nature (London) **574**, 505 (2019).

[2] P. Ball, First 100-qubit quantum computer enters crowded race, Nature (London) **599**, 542 (2021).

[3] J. Preskill, Quantum computing in the NISQ era and beyond, Quantum **2**, 79 (2018).

[4] S. McArdle, S. Endo, A. Aspuru-Guzik, S. C. Benjamin, and X. Yuan, Quantum computational chemistry, Rev. Mod. Phys. **92**, 015003 (2020).

[5] S. Endo, Z. Cai, S. C. Benjamin, and X. Yuan, Hybrid quantum-classical algorithms and quantum error mitigation, J. Phys. Soc. Jpn. **90**, 032001 (2021).

[6] M. Cerezo, A. Arrasmith, R. Babbush, S. C. Benjamin, S. Endo, K. Fujii, J. R. McClean, K. Mitarai, X. Yuan, L. Cincio, and P. J. Coles, Variational quantum algorithms, Nat. Rev. Phys. **3**, 625 (2021).

[7] K. Bharti, A. Cervera-Lierta, T. H. Kyaw, T. Haug, S. Alperin-Lea, A. Anand, M. Degroote, H. Heimonen, J. S. Kottmann, T. Menke, W.-K. Mok, S. Sim, L.-C. Kwek, and A. Aspuru-Guzik, Noisy intermediate-scale quantum algorithms, Rev. Mod. Phys. **94**, 015004 (2022).

[8] A. Peruzzo, J. McClean, P. Shadbolt, M.-H. Yung, X.-Q. Zhou, P. J. Love, A. Aspuru-Guzik, and J. L. Obrien, A variational eigenvalue solver on a photonic quantum processor, Nat. Commun. **5**, 4213 (2014).

[9] J. R. McClean, J. Romero, R. Babbush, and A. Aspuru-Guzik, The theory of variational hybrid quantum-classical algorithms, New J. Phys. **18**, 023023 (2016).

[10] E. Farhi, J. Goldstone, and S. Gutmann, A quantum approximate optimization algorithm, arXiv:1411.4028.

[11] K. Mitarai, M. Negoro, M. Kitagawa, and K. Fujii, Quantum circuit learning, Phys. Rev. A **98**, 032309 (2018).

[12] E. Farhi and H. Neven, Classification with quantum neural networks on near term processors, arXiv:1802.06002.

[13] V. Havlíček, A. D. Córcoles, K. Temme, A. W. Harrow, A. Kandala, J. M. Chow, and J. M. Gambetta, Supervised learning with quantum-enhanced feature spaces, Nature (London) **567**, 209 (2019).

[14] T. Kusumoto, K. Mitarai, K. Fujii, M. Kitagawa, and M. Negoro, Experimental quantum kernel trick with nuclear spins in a solid, npj Quantum Inf. **7**, 94 (2021).

[15] M. Schuld and N. Killoran, Quantum machine learning in feature hilbert spaces, Phys. Rev. Lett. **122**, 040504 (2019).

[16] M. Benedetti, E. Lloyd, S. Sack, and M. Fiorentini, Parameterized quantum circuits as machine learning models, Quantum Sci. Technol. **4**, 043001 (2019).

[17] P. J. J. OMalley, R. Babbush, I. D. Kivlichan, J. Romero, J. R. McClean, R. Barends, J. Kelly, P. Roushan, A. Tranter, N. Ding, B. Campbell, Y. Chen, Z. Chen, B. Chiaro, A. Dunsworth, A. G. Fowler, E. Jeffrey, E. Lucero, A. Megrant, J. Y. Mutus *et al.*,

Scalable quantum simulation of molecular energies, Phys. Rev. X **6**, 031007 (2016).

[18] A. Kandala, A. Mezzacapo, K. Temme, M. Takita, M. Brink, J. M. Chow, and J. M. Gambetta, Hardware-efficient variational quantum eigensolver for small molecules and quantum magnets, Nature (London) **549**, 242 (2017).

[19] J. I. Colless, V. V. Ramasesh, D. Dahlen, M. S. Blok, M. E. Kimchi-Schwartz, J. R. McClean, J. Carter, W. A. de Jong, and I. Siddiqi, Computation of molecular spectra on a quantum processor with an error-resilient algorithm, Phys. Rev. X **8**, 011021 (2018).

[20] A. Kandala, K. Temme, A. D. Córcoles, A. Mezzacapo, J. M. Chow, and J. M. Gambetta, Error mitigation extends the computational reach of a noisy quantum processor, Nature (London) **567**, 491 (2019).

[21] Y. Shen, X. Zhang, S. Zhang, J.-N. Zhang, M.-H. Yung, and K. Kim, Quantum implementation of the unitary coupled cluster for simulating molecular electronic structure, Phys. Rev. A **95**, 020501(R) (2017).

[22] C. Hempel, C. Maier, J. Romero, J. McClean, T. Monz, H. Shen, P. Jurcevic, B. P. Lanyon, P. Love, R. Babbush, A. Aspuru-Guzik, R. Blatt, and C. F. Roos, Quantum chemistry calculations on a trapped-ion quantum simulator, Phys. Rev. X **8**, 031022 (2018).

[23] C. Kokail, C. Maier, R. van Bijnen, T. Brydges, M. K. Joshi, P. Jurcevic, C. A. Muschik, P. Silvi, R. Blatt, C. F. Roos, and P. Zoller, Self-verifying variational quantum simulation of lattice models, Nature (London) **569**, 355 (2019).

[24] Y. Nam, J.-S. Chen, N. C. Pisenti, K. Wright, C. Delaney, D. Maslov, K. R. Brown, S. Allen, J. M. Amini, J. Apisdorf, K. M. Beck, A. Blinov, V. Chaplin, M. Chmielewski, C. Collins, S. Debnath, K. M. Hudek, A. M. Ducore, M. Keesan, S. M. Kreikemeier *et al.*, Ground-state energy estimation of the water molecule on a trapped-ion quantum computer, npj Quantum Inf. **6**, 33 (2020).

[25] D. Wecker, M. B. Hastings, and M. Troyer, Progress towards practical quantum variational algorithms, Phys. Rev. A **92**, 042303 (2015).

[26] W. J. Huggins, J. R. McClean, N. C. Rubin, Z. Jiang, N. Wiebe, K. B. Whaley, and R. Babbush, Efficient and noise resilient measurements for quantum chemistry on near-term quantum computers, npj Quantum Inf. **7**, 23 (2021).

[27] J. F. Gonthier, M. D. Radin, C. Buda, E. J. Doskocil, C. M. Abuan, and J. Romero, Measurements as a roadblock to near-term practical quantum advantage in chemistry: Resource analysis, Phys. Rev. Res. **4**, 033154 (2022).

[28] J. Tilly, H. Chen, S. Cao, D. Picozzi, K. Setia, Y. Li, E. Grant, L. Wossnig, I. Rungger, G. H. Booth, and J. Tennyson, The variational quantum eigensolver: A review of methods and best practices, Phys. Rep. **986**, 1 (2022).

[29] W. Saib, P. Wallden, and I. Akhalwaya, The effect of noise on the performance of variational algorithms for quantum chemistry, in *Proceedings of the 2021 IEEE International Conference on Quantum Computing and Engineering (QCE), Broomfield, CO* (IEEE, 2021), pp. 42–53.

[30] I. Miháliková, M. Pivoluska, M. Plesch, M. Friák, D. Nagaj, and M. Šob, The cost of improving the precision of the variational quantum eigensolver for quantum chemistry, Nanomaterials **12**, 243 (2022).

[31] W. Sennane, J.-P. Piquemal, and M. J. Rančić, Calculating the ground-state energy of benzene under spatial deformations with noisy quantum computing, Phys. Rev. A **107**, 012416 (2023).

[32] M. Oliv, A. Matic, T. Messerer, and J. M. Lorenz, Evaluating the impact of noise on the performance of the variational quantum eigensolver, arXiv:2209.12803.

[33] E. Fontana, N. Fitzpatrick, D. M. Ramo, R. Duncan, and I. Rungger, Evaluating the noise resilience of variational quantum algorithms, Phys. Rev. A **104**, 022403 (2021).

[34] Y. Li and S. C. Benjamin, Efficient variational quantum simulator incorporating active error minimization, Phys. Rev. X **7**, 021050 (2017).

[35] K. Temme, S. Bravyi, and J. M. Gambetta, Error mitigation for short-depth quantum circuits, Phys. Rev. Lett. **119**, 180509 (2017).

[36] S. Endo, S. C. Benjamin, and Y. Li, Practical quantum error mitigation for near-future applications, Phys. Rev. X **8**, 031027 (2018).

[37] J. R. McClean, M. E. Kimchi-Schwartz, J. Carter, and W. A. de Jong, Hybrid quantum-classical hierarchy for mitigation of decoherence and determination of excited states, Phys. Rev. A **95**, 042308 (2017).

[38] X. Bonet-Monroig, R. Sagastizabal, M. Singh, and T. E. O'Brien, Low-cost error mitigation by symmetry verification, Phys. Rev. A **98**, 062339 (2018).

[39] S. McArdle, X. Yuan, and S. Benjamin, Error-mitigated digital quantum simulation, Phys. Rev. Lett. **122**, 180501 (2019).

[40] Y. Chen, M. Farahzad, S. Yoo, and T.-C. Wei, Detector tomography on IBM quantum computers and mitigation of an imperfect measurement, Phys. Rev. A **100**, 052315 (2019).

[41] F. B. Maciejewski, Z. Zimborás, and M. Oszmaniec, Mitigation of readout noise in near-term quantum devices by classical post-processing based on detector tomography, Quantum **4**, 257 (2020).

[42] H. Kwon and J. Bae, A hybrid quantum-classical approach to mitigating measurement errors in quantum algorithms, IEEE Trans. Comput. **70**, 1401 (2021).

[43] A. Strikis, D. Qin, Y. Chen, S. C. Benjamin, and Y. Li, Learning-based quantum error mitigation, PRX Quantum **2**, 040330 (2021).

[44] P. Czarnik, A. Arrasmith, P. J. Coles, and L. Cincio, Error mitigation with Clifford quantum-circuit data, Quantum **5**, 592 (2021).

[45] M. S. Rudolph, J. Miller, J. Chen, A. Acharya, and A. Perdomo-Ortiz, Synergy between quantum circuits and tensor networks: Short-cutting the race to practical quantum advantage, arXiv:2208.13673.

[46] A. Cervera-Lierta, J. S. Kottmann, and A. Aspuru-Guzik, Meta-variational quantum eigensolver: Learning energy profiles of parameterized Hamiltonians for quantum simulation, PRX Quantum **2**, 020329 (2021).

[47] J. Ceroni, T. F. Stetina, M. Kieferova, C. O. Marrero, J. M. Arrazola, and N. Wiebe, Generating approximate ground states of molecules using quantum machine learning, arXiv:2210.05489.

[48] J. S. Kottmann and A. Aspuru-Guzik, Optimized low-depth quantum circuits for molecular electronic structure using a separable-pair approximation, Phys. Rev. A **105**, 032449 (2022).

[49] K. Fujii, K. Mizuta, H. Ueda, K. Mitarai, W. Mizukami, and Y. O. Nakagawa, Deep variational quantum eigensolver: A divide-and-conquer method for solving a larger problem with smaller size quantum computers, PRX Quantum **3**, 010346 (2022).

[50] S. Bravyi, D. Gosset, and R. Movassagh, Classical algorithms for quantum mean values, Nat. Phys. **17**, 337 (2021).

[51] X. G. Wen, Topological orders in rigid states, Int. J. Mod. Phys. B **04**, 239 (1990).

[52] Z.-C. Gu and X.-G. Wen, Tensor-entanglement-filtering renormalization approach and symmetry-protected topological order, Phys. Rev. B **80**, 155131 (2009).

[53] F. Pollmann, E. Berg, A. M. Turner, and M. Oshikawa, Symmetry protection of topological phases in one-dimensional quantum spin systems, Phys. Rev. B **85**, 075125 (2012).

[54] Y. Yang, Z.-Z. Sun, S.-J. Ran, and G. Su, Visualizing quantum phases and identifying quantum phase transitions by nonlinear dimensional reduction, Phys. Rev. B **103**, 075106 (2021).

[55] A. C. Doherty and S. D. Bartlett, Identifying phases of quantum many-body systems that are universal for quantum computation, Phys. Rev. Lett. **103**, 020506 (2009).

[56] I. Cong, S. Choi, and M. D. Lukin, Quantum convolutional neural networks, Nat. Phys. **15**, 1273 (2019).

[57] S. Trebst, P. Werner, M. Troyer, K. Shtengel, and C. Nayak, Breakdown of a topological phase: Quantum phase transition in a loop gas model with tension, Phys. Rev. Lett. **98**, 070602 (2007).

[58] H. W. J. Blöte and Y. Deng, Cluster Monte Carlo simulation of the transverse Ising model, Phys. Rev. E **66**, 066110 (2002).

[59] F. Wu, Y. Deng, and N. Prokof'ev, Phase diagram of the toric code model in a parallel magnetic field, Phys. Rev. B **85**, 195104 (2012).

[60] T. Sancho-Lorente, J. Román-Roche, and D. Zueco, Quantum kernels to learn the phases of quantum matter, Phys. Rev. A **105**, 042432 (2022).

[61] Y. Wu, B. Wu, J. Wang, and X. Yuan, Quantum phase recognition via quantum kernel methods, Quantum **7**, 981 (2023).

[62] H. T. Quan, Z. Song, X. F. Liu, P. Zanardi, and C. P. Sun, Decay of Loschmidt echo enhanced by quantum criticality, Phys. Rev. Lett. **96**, 140604 (2006).

[63] P. Zanardi and N. Paunković, Ground state overlap and quantum phase transitions, Phys. Rev. E **74**, 031123 (2006).

[64] R. Raussendorf and H. J. Briegel, A one-way quantum computer, Phys. Rev. Lett. **86**, 5188 (2001).

[65] R. Raussendorf, D. E. Browne, and H. J. Briegel, Measurement-based quantum computation on cluster states, Phys. Rev. A **68**, 022312 (2003).

[66] Y. Suzuki, Y. Kawase, Y. Masumura, Y. Hiraga, M. Nakadai, J. Chen, K. M. Nakanishi, K. Mitarai, R. Imai, S. Tamiya, T. Yamamoto, T. Yan, T. Kawakubo, Y. O. Nakagawa, Y. Ibe, Y. Zhang, H. Yamashita, H. Yoshimura, A. Hayashi, and K. Fujii, Qulacs: A fast and versatile quantum circuit simulator for research purpose, Quantum **5**, 559 (2021).

[67] P. Virtanen, R. Gommers, T. E. Oliphant, M. Haberland, T. Reddy, D. Cournapeau, E. Burovski, P. Peterson, W. Weckesser, J. Bright, S. J. van der Walt, M. Brett, J. Wilson, K. J. Millman, N. Mayorov, A. R. J. Nelson, E. Jones, R. Kern, E. Larson, C. J. Carey *et al.*, SciPy 1.0: Fundamental algorithms for scientific computing in Python, Nat. Methods **17**, 261 (2020).

[68] F. Pedregosa, G. Varoquaux, A. Gramfort, V. Michel, B. Thirion, O. Grisel, M. Blondel, P. Prettenhofer, R. Weiss, V. Dubourg, J. Vanderplas, A. Passos, D. Cournapeau, M. Brucher, M. Perrot, and É. Duchesnay, Scikit-learn: Machine learning in Python, J. Mach. Learn. Res. **12**, 2825 (2011).

[69] H.-Q. Zhou and J. P. Barjaktarevi, Fidelity and quantum phase transitions, J. Phys. A **41**, 412001 (2008).

[70] H.-Q. Zhou, J.-H. Zhao, and B. Li, Fidelity approach to quantum phase transitions: finite-size scaling for the quantum Ising model in a transverse field, J. Phys. A **41**, 492002 (2008).

[71] W.-L. You, Y.-W. Li, and S.-J. Gu, Fidelity, dynamic structure factor, and susceptibility in critical phenomena, Phys. Rev. E **76**, 022101 (2007).

[72] P. W. Anderson, Infrared catastrophe in Fermi gases with local scattering potentials, Phys. Rev. Lett. **18**, 1049 (1967).

[73] G. Evenbly and G. Vidal, Class of highly entangled many-body states that can be efficiently simulated, Phys. Rev. Lett. **112**, 240502 (2014).

[74] J. Yu, S.-P. Kou, and X.-G. Wen, Topological quantum phase transition in the transverse Wen-plaquette model, Europhys. Lett. **84**, 17004 (2008).

[75] R. Li, B. Wu, M. Ying, X. Sun, and G. Yang, Quantum supremacy circuit simulation on Sunway TaihuLight, IEEE Trans. Parallel Distrib. Syst. **31**, 805 (2020).

[76] S. Boixo, S. V. Isakov, V. N. Smelyanskiy, and H. Neven, Simulation of low-depth quantum circuits as complex undirected graphical models, arXiv:1712.05384.

[77] C. Guo, Y. Liu, M. Xiong, S. Xue, X. Fu, A. Huang, X. Qiang, P. Xu, J. Liu, S. Zheng, H.-L. Huang, M. Deng, D. Poletti, W.-S. Bao, and J. Wu, General-purpose quantum circuit simulator with projected entangled-pair states and the quantum supremacy frontier, Phys. Rev. Lett. **123**, 190501 (2019).

[78] J. Chen, F. Zhang, C. Huang, M. Newman, and Y. Shi, Classical simulation of intermediate-size quantum circuits, arXiv:1805.01450.

[79] F. Pan, P. Zhou, S. Li, and P. Zhang, Contracting arbitrary tensor networks: General approximate algorithm and applications in graphical models and quantum circuit simulations, Phys. Rev. Lett. **125**, 060503 (2020).

[80] C. Guo, Y. Zhao, and H.-L. Huang, Verifying random quantum circuits with arbitrary geometry using tensor network states algorithm, Phys. Rev. Lett. **126**, 070502 (2021).

[81] F. Pan and P. Zhang, Simulation of quantum circuits using the big-batch tensor network method, Phys. Rev. Lett. **128**, 030501 (2022).